Raytheon

Pulsed Doppler Lidar Airborne Scanner

Progress Report No. 35
January - September 1985

Prepared for

George C. Marshall Space Flight Center
NASA
Huntsville, Alabama 35812

Prepared by

C. A. DiMarzio
D. B. McVicker
C. E. Morrow
C. C. Negus

Raytheon Company
Equipment Development Laboratories
Electro-Optics Systems Laboratory
Sudbury, Massachusetts 01776

Contract No. NAS8-33120

ER85-4352

10 October 1985

32+2

Raytheon

Pulsed Doppler Lidar Airborne Scanner

Progress Report No. 35
January - September 1985

Prepared for

George C. Marshall Space Flight Center
NASA
Huntsville, Alabama 35812

Prepared by

C. A. DiMarzio
D. B. McVicker
C. E. Morrow
C. C. Negus

Raytheon Company
Equipment Development Laboratories
Electro-Optics Systems Laboratory
Sudbury, Massachusetts 01776

Contract No. NAS8-33120

ER85-4352

10 October 1985

1. INTRODUCTION

This report covers the work accomplished during the reporting period on the subject contract and describes plans for the next reporting period. The objectives during the current phase of the contract are divided into four phases. Phase 1 includes ground testing of the system and analysis of data from the 1981 Severe Storms Test Flights. Phase 2 consists of preflight preparation and planning for the 1983 flight series. The flight test itself will be performed during Phase 3, and Phase 4 consists of post-flight analysis and operation of the system after that flight test.

Section 2 describes the work performed during the present reporting period, and Section 3 provides plans for the next reporting period.

2. WORK PERFORMED

2.1 DATA ANALYSIS

2.1.1 RANGE PERFORMANCE AGAINST DIFFERENT TARGETS

Figure 1 shows the range profile from five samples taken during Flight 10, around 1700 Z. The lowest curve is taken from data collected upwind of Mt. Shasta at about 10,000 feet of altitude, in a clear atmosphere, where no signals were observed. It thus is a good representation of the noise level as a function of range. The next curve was taken downwind of the mountain, and shows evidence of atmospheric returns. There is some question as to whether the data are valid at all ranges, or some ranges are contaminated by the others.

The top three curves show the returns from Mt. Shasta at 8 to 10 kilometers. These demonstrate several features of the time history of the pulse. There is a "shelf" about 3 kilometers long, 9 dB below the peak of the pulse, and ringing after the pulse with a peak about 12 dB below the level of the pulse with a decay time of 33 microseconds and a period of almost 1 kilometer (6.7 microseconds) corresponding to a frequency of 150 kHz. The ringing does not decay to zero, but is still some 5 dB above the noise at the end of 200 microseconds.

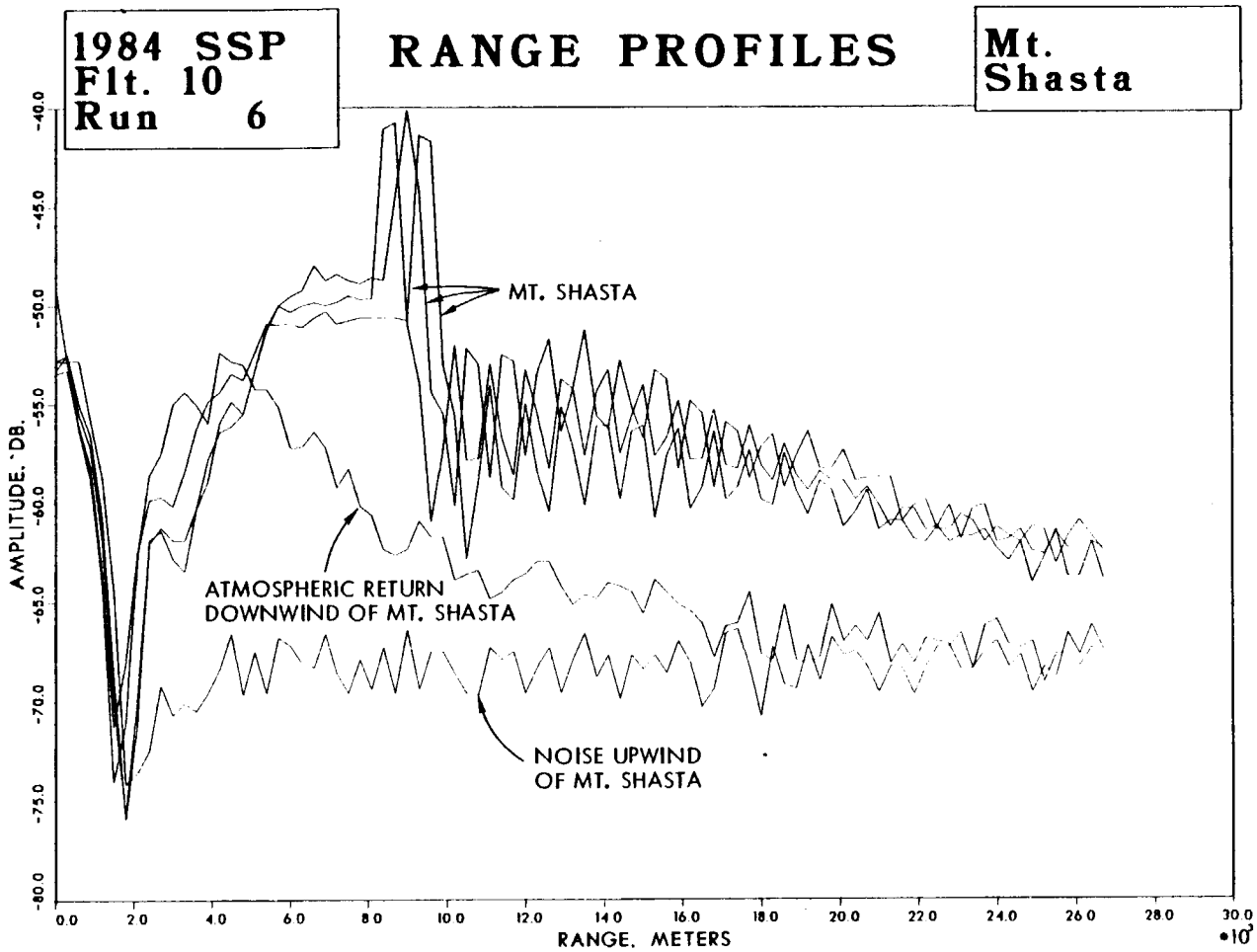

Figure 1. Range Profiles from Flight 10, 1984 SSP

2.1.2 ANALYSIS OF PULSE SHAPE

	Det. Level mV	Time μsec	Equiv. Range km	Rel. Power dB	Rel. Energy per Gate dB	Total Rel. Energy dB
Pulse Start	142	0	0	0		
End	78	2	-0.3	- 2.6	0	0
Tail Start	78	2	-0.3	- 2.6	- 2.6	
End	0	4	-0.6			-4.5
Shelf Start	0	-78	11.7			
End	14	0	0	-10.0	- 9.0	3.9
Ringing Start	6	4	-0.6	-13.7	-12.6	
Half	3	24	-3.6	-16.8	-15.6	
1/e	2.2	33	-4.9	-18.1	-17.0	
Total*						-4.0

* Average over Peaks + Nulls

Photographs of the pulse shape were taken by placing the Rockwell detector in front of the telescope with an aperture of a few millimeters and connecting the detector to an oscilloscope. The two channels of the scope were connected together to increase the gain, so that the pulse peak and the power before and after it were measurable. Several photos were taken with different vertical and horizontal scales and with different delays, to provide a time history of the entire pulse. These are shown in Figure 2. The center photo shows the entire time history. In this case, the pulse is barely visible in the third major box from the left. The lower two photos expand the regions before and after the pulse, and the top photo shows the detail of the pulse itself.

The above table shows the results of analysis of the photographs of the pulse shape. The photos are considered to be divided into four parts. The first is the "shelf" which precedes the pulse. This occurs because the amplifiers are turned on prior to the optical pulse, in order to generate the

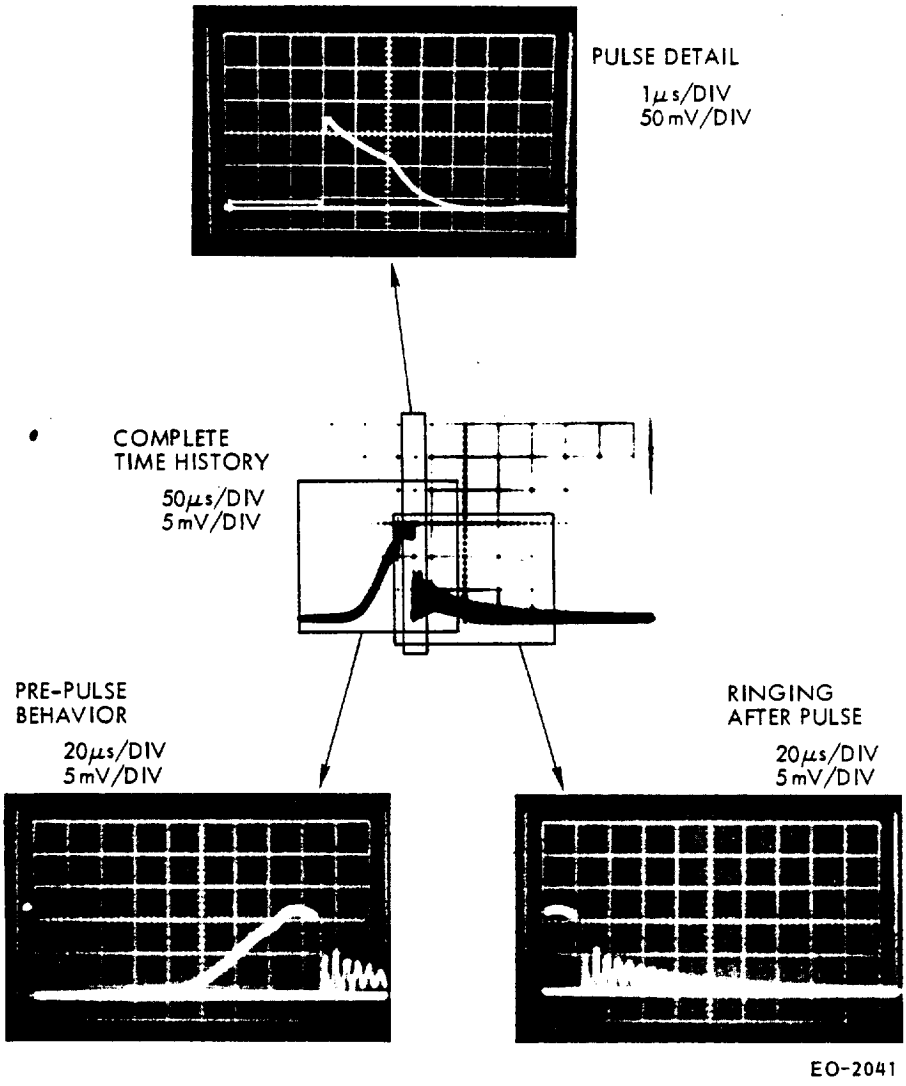

Figure 2. Pulse Shape Photos Taken at MSFC in January 1985

required gain. Unfortunately, this gain also amplifies the leakage through the modulator. The shelf is described to a first approximation as being triangular, and the table shows the start and end of the shelf.

The second region is the pulse itself, which is again described in trapezoidal approximation. The details of this region were taken from the top photograph. The third region is the tail of the pulse, before the ringing begins to be noticeable.

Finally, the ringing region is considered. This region is caused by mechanical ringing of the modulator, and is characterized by sinusoidal modulation at a frequency of 150 kHz, which has a period of 6.6 microseconds, corresponding to 990 meters of range. The envelope of the ringing is described by an exponential function, with the decay time calculated by measuring the time required to decay to half-height. The total energy is obtained by dividing the integral of the power envelope by two to account for averaging over many cycles.

The immediate conclusions of this analysis are that the shelf can contribute to a spurious signal at a range before a hard target if the signal from that target is more than 9 dB above the noise. Furthermore, it will contribute a false velocity in this region if the hard target signal is more than 9 dB above the atmospheric signal from a range gate in the region. Finally, it will cause a similar effect in atmospheric signals if there are about eight or more range gates beyond the one being considered which have signals comparable to the current one. The total energy of 3.9 dB above the energy in the signal pulse means that in many cases, the signal will be corrupted by energy from this region.

These conditions also hold for the ringing, except that the signals will be corrupted at ranges beyond the source of the signal rather than before it, and the magnitude of the effect will be smaller because of the lower powers and energies in this region.

Application of these results to specific atmospheric measurements will be the subject of later work.

Figure 3 shows the amplitude as a function of location for two forward and two aft scans. The flight path was from left to right, across the bottom of the plot. The ambient wind was from right to left at about 220 degrees relative to true north. It is evident that the atmosphere was clean and that no signals were detected upwind of the mountain. The strong mountain returns are visible about a quarter of the way from the right-hand edge of the pictures. Note that increasing darkness indicates increasing amplitude. The shelf before the pulse and the ringing afterward are clearly evident. Before the mountain signals are observed, there is an increase in the signal at near ranges, apparently due to increased backscatter in the air which has passed over and around the mountain. It appears that this occurs at progressively shorter ranges as the aircraft approached the mountain, and that the air became too clean to provide a signal, somewhere abreast of the mountain. The aft scans show a similar behavior. In addition, several scans are contaminated by strong ground returns at long ranges.

Figure 4 shows the corresponding velocity plots. At the ranges where the intensities are enhanced, upwind (left) of the mountain, there are variations in the velocity component which may be attributed to a wake caused by the mountain. When the mountain is visible in the scan, the velocity of the mountain is normally obtained at all ranges. This velocity has been examined in printouts of the data, and found to be within half a meter per second of zero. Lighter colors represent approaching (positive) velocities and darker ones represent receding velocities. The velocities were obtained from the VELOCITY data by changing the sign on the forward scans only, and adding the value of OFFSET.

2.1.3 DECONVOLUTION OF RANGE DATA

One of the major deficiencies of data collected during the 1984 flight tests is the existence of spurious data due to the failure of the electro-optic modulator. It is believed that a large number of the measured velocities are still valid, and that deconvolution techniques may be used to determine the data validity, thereby making most of this data usable for meteorological studies.

Figure 3. Scalar Plots of Amplitude for Flight 10 1984 SSP

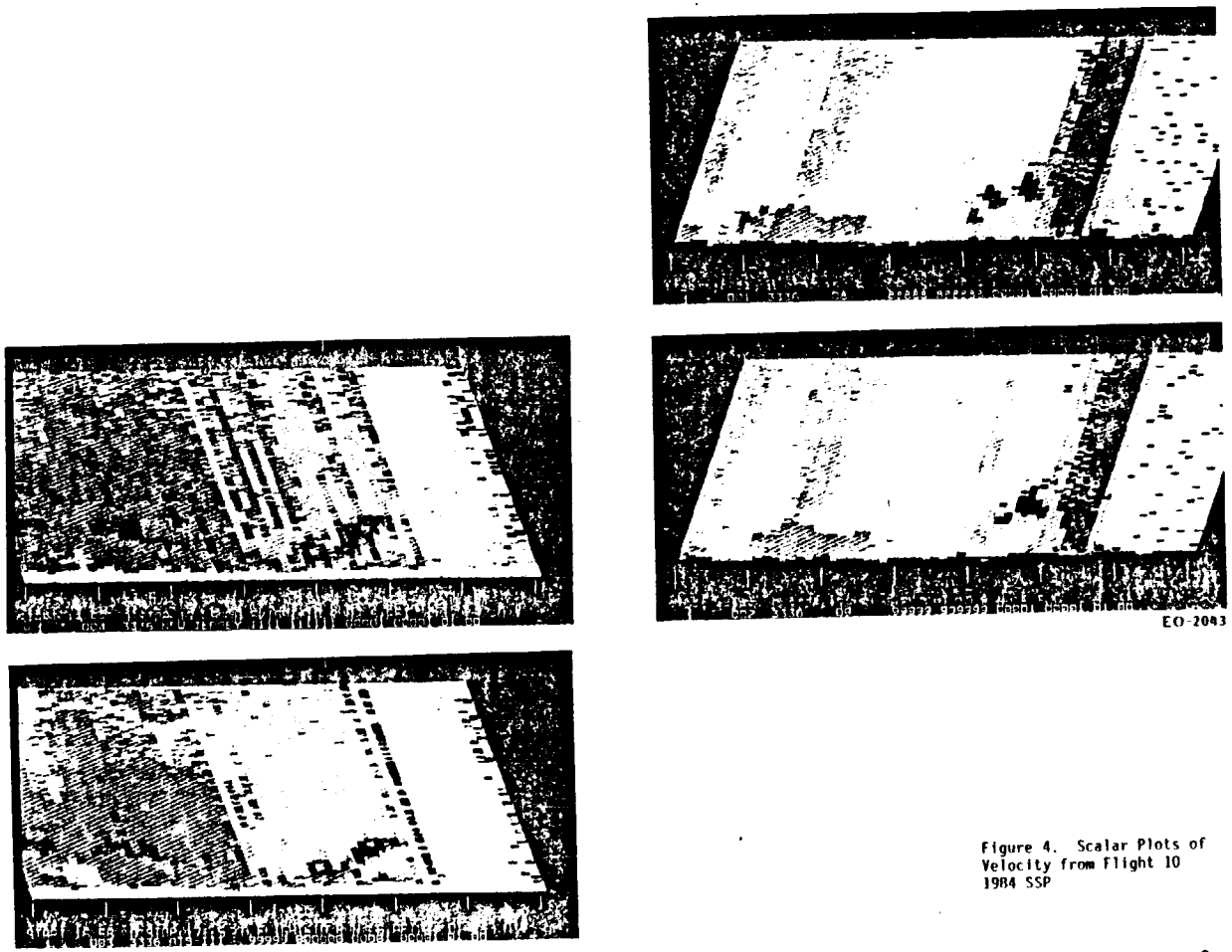

Figure 4. Scalar Plots of Velocity from Flight 10 1984 SSP

The problem may be summarized as follows: in normal operation, the lidar is a pulsed Doppler lidar, and returns processed in a particular range gate (a given time interval after the transmitter pulse) may be unambiguously associated with a range from the sensor determined by the given round-trip transit time. After the failure of the electro-optic modulator, a substantial amount of energy was transmitted both before and after the main pulse. Thus, in any range gate, the return signal is a sum of contributions from different ranges along the line of sight. In particular, at longer ranges where it is anticipated that there is no useful signal, contributions from the closer ranges, resulting from energy transmitted after the pulse, will often produce an apparent signal. The problem then is to determine how far out in range this signal is to be believed.

The deconvolution techniques to be described below offer hope for resolving some of these questions. If full spectral data were available, it would be possible to perform a complete deconvolution and recover almost all of the lost information. However, in the system as it was used in 1984, only spectral parameters are available. Nevertheless, it is still possible to recover a considerable amount of useful information from careful evaluation of these parameters as functions of range. The approach involves making assumption about the missing spectral information on the basis of available parameters. In this way, it is possible to establish varying degrees of confidence in the deconvolved data at different ranges.

2.1.4 DERIVATION OF THE CONVOLUTION EXPRESSION

The signal-to-noise ratio at any point in time after the transmitted pulse is an integral of contributions over all ranges from 0 to infinity. The average signal-to-noise ratio in a particular range gate is the average of the signal-to-noise ratio over that particular range gate. This can be represented by the following equation, as shown in Figure 5.

$$\overline{SNR}_m = \frac{1}{T} \int_{t_g - \frac{T}{2}}^{t_g - \frac{T}{2}} \int_0^{\infty} \frac{\eta P(\tau_t)}{h\nu B} \frac{dF(\rho)}{d\rho} \, d\rho \, d\tau_g \qquad (1)$$

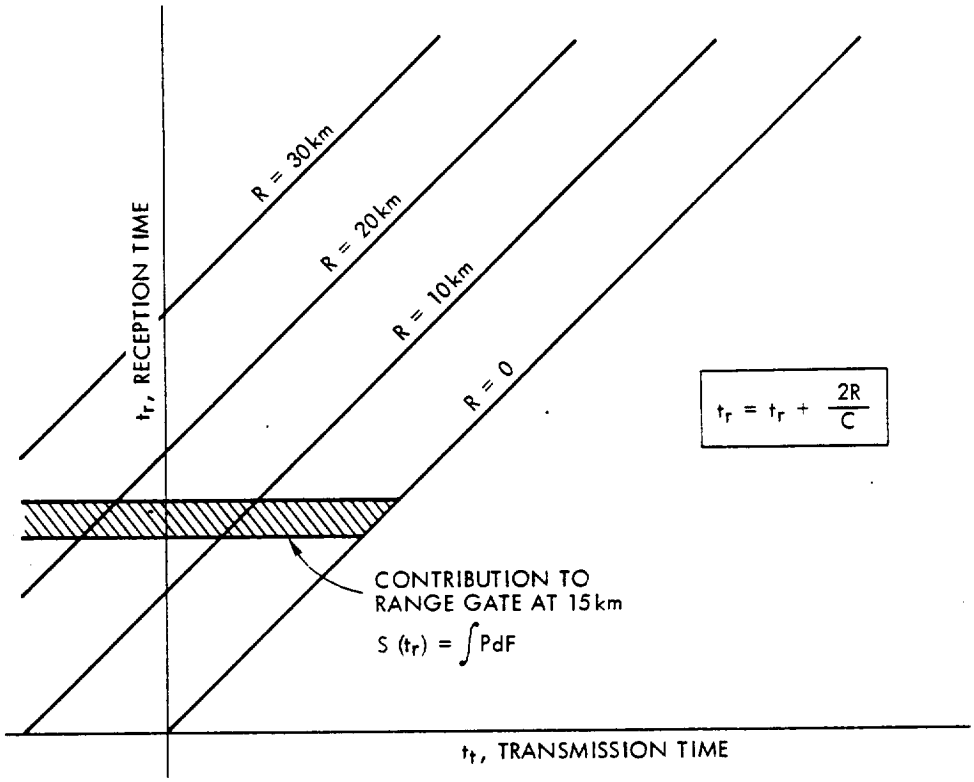

P IS THE TRANSMITTER POWER AT TIME $t_r - \frac{2R}{C}$

F IS THE HETERODYNE COLLECTION FACTOR

$$dF = \frac{\lambda b}{R^2+b^2}\ \beta(\pi)\ dR\ 10^{-2\alpha R/10}$$

b = RAYLEIGH RANGE = 3023 METERS

α = ATTENUATION COEFFICIENT, dB/km

$\beta(\pi)$ = BACKSCATTER COEFFICIENT, $m^{-1}sr^{-1}$

EOA-4705

Figure 5. Calculating the Contribution to a Range Gate

where T is the duration of a range gate,

η is the overall system efficiency,

$P(\tau_t)$ is the power transmitted, which is a function of the time at which it was transmitted,

$h\nu$ is the energy of a photon,

B is the bandwidth,

$F(\rho)$ is the fraction of the transmitted power which is returned in such a way as to mix efficiently with the local oscillator,

ρ is the range, and

τ_g is the time associated with the center of the range gate.

It will be noted that the two times and the range in the above equation are related as follows:

$$\tau_t = \tau_g - \frac{2\rho}{c} \tag{2}$$

The integral over range may be broken up into a sum of integrals over small segments. Later it will be convenient to make each of these segments correspond to a range increment equivalent to the time interval of the range gate. The resulting equation is shown here:

$$\overline{SNR_m} = \sum_{n_R=0}^{\infty} \int_{t_g - \frac{T}{2}}^{t_g + \frac{T}{2}} \int_{R - \frac{\Delta R}{2}}^{R + \frac{\Delta R}{2}} \frac{\eta P\left(t_g + \tau_g \frac{2(R+\rho)}{c}\right)}{h\nu BT} \frac{dF(R+\rho)}{d\rho} \, d\rho \, d\tau_g \tag{3}$$

where t_g is the time associated with the center of the range gate, and

R is the range associated with the center of the range increment.

One may then conveniently define the average energy as follows:

$$\bar{E} = \frac{1}{\Delta R} \int_{-\frac{T}{2}}^{\frac{T}{2}} \int_{-\frac{\Delta R}{2}}^{\frac{\Delta R}{2}} \rho\left(t_g + \tau_g - \frac{2(R+\rho)}{c}\right) d\rho \, d\tau_g \tag{4}$$

and a weighted average signal-to-noise ratio contribution from the range R as;

$$\overline{SNR_C} = \int_{-\frac{T}{2}}^{\frac{T}{2}} \int_{-\frac{\Delta R}{2}}^{\frac{\Delta R}{2}} \frac{\eta P\left(t_g + \tau_g - 2\frac{(R+\rho)}{c}\right)}{h\nu BT} \frac{dF(R+\rho)}{d\rho} \, d\rho \, d\tau_g \qquad (5)$$

With this definition then, the measured signal-to-noise ratio is related to the signal-to-noise ratio contributions by the following equation,

$$\overline{SNR_m} = \sum_{n=0}^{\infty} \frac{\overline{E}}{E} \overline{SNR_C} \quad (R_n) \qquad (6)$$

This equation relates the measured signal-to-noise ratio in a particular range gate to the contributions from all different ranges, weighted with the appropriate transmitter energy. It may be expressed in matrix form as follows:

$$\overline{M} = \underline{\underline{E}} \; \overline{C} \qquad (7)$$

In this case, $\overline{C}$ is a column matrix in which each element is the signal-to-noise ratio contribution for a particular interval, starting with the closest and continuing to the furthest. Likewise, $\overline{M}$ is a column matrix whose elements are the measured signal-to-noise ratios in each of the range gates sequentially. The matrix $\underline{\underline{E}}$ consists of the elements $\overline{E}/E$. Each of these elements is defined as shown below:

$$\begin{aligned} m_i &= \overline{SNR_m}\,(t_g = i\Delta t) \\ c_j &= \overline{SNR_C} \quad R = j\frac{C\Delta t}{2} \\ e_{ij} &= \frac{\overline{E}}{E} \quad \left(t_t = (i-j)\,\Delta t\right) \end{aligned} \qquad (8)$$

2.1.5 CONVOLUTION

The simple expression developed in the above section suggests the approach of inverting the matrix $\underline{\underline{E}}$, thereby solving for the SNR contributions in terms of the measured values;

$$\bar{C} = \underline{\underline{E}}^{-1} \bar{M} \tag{9}$$

It can be shown that this is mathematically equivalent to the process of deconvolution, which is often accomplished by taking the Fourier transform of the measured data and that of the convolving function, dividing the former by the latter, and taking the inverse Fourier transform. This provides an extremely straightforward method for extracting information where the intensity of a signal is a convolution along the line of sight of the desired function and the transmitter energy time history. All that is necessary is to calculate the matrix elements of $\underline{\underline{E}}$ from the known transmitter time history. The resulting matrix may then be inverted and used to convert any measured data set to the desired output.

In the case of the Doppler lidar, the convolution process applies to the signals obtained at each Doppler frequency. In the present system, complete spectral data are not available. The signal processor examines the spectrum which arises from the convolutions described above, and extracts the amplitude and Doppler frequency associated with the spectral peak. Thus, no information is available concerning the amplitude of frequencies other than that associated with the peak. One exception which will prove useful later on is the fact that it is known that all of these amplitudes must be less than or equal to the peak one.

This fact may be applied in the following way. The matrix of measured data, $\bar{M}$, for a specified Doppler frequency may be divided into two parts: the known part and the unknown part. The known part, $\underline{M}_k$, consists of elements whose value is equal to the measured amplitude in just those range gates in which the Doppler velocity under consideration is the one actually measured. The remaining elements are all zero. Conversely, the unknown part, $\underline{M}_u$, consists of all zeros where the matrix $\underline{M}_k$ has non-zero values, and vice versa. The remaining question is what values to use for these non-zero elements of $\underline{M}_u$. We will examine these in terms of their effect on the desired output. It is known that all of these non-zero elements must be non-negative since they represent measurements of energy in the receiver, and it is also known that the elements of $\underline{\underline{E}}^{-1}$ may be either positive or negative. Thus the effect of an element of $\bar{M}_u$ on an element of the output, $\bar{C}$, may be to increase it or decrease it. The maximum

value of an element of $\bar{C}$ will be achieved when $\bar{M}_u$ has large positive values in just those cases where they will be multiplied by positive elements of $\underline{\underline{E}}$, and zero elsewhere. Of course, the maximum value which an element of $\bar{M}_u$ may have is simply the measured signal in the corresponding range gate, since if it were any higher, it would become the new peak in the spectrum. This condition may be simulated by extracting from $\underline{\underline{E}}^{-1}$ the positive elements, setting the negative elements to zero, in a new matrix $\underline{\underline{E}}_+^{-1}$. The maximum value which an element of $\bar{C}$ may assume is then obtained by adding the value calculated by this matrix and the unknown measurements to calculate with the complete E^{-1} matrix and the known elements;

$$\bar{C}_T = \underline{\underline{E}}^{-1} \bar{M}_k + \underline{\underline{E}}_+^{-1} \bar{M}_u \tag{10}$$

Likewise, the maximum value of an element of $\bar{C}$ is achieved when the unknown data points are at their maximum value in just those cases where they will be multiplied by negative elements of $\underline{\underline{E}}^{-1}$. This may be achieved mathematically in an analagous fashion to Equation 11, with the following results:

$$\bar{C}_N = \underline{\underline{E}}^{-1} \bar{M}_k - \underline{\underline{E}}_-^{-1} \bar{M}_u \tag{11}$$

Having performed the calculations indicated by Equations 9, 10 and 11, one obtains three values of the signal contribution for each velocity and each range gate. Comparisons among these values may be expected to yield a best estimate of the velocity at each range, along with at least a qualitative evaluation of its validity.

2.1.6 TEST RESULTS

The procedures described above have been implemented on a few sets of data from the 1984 Severe Storms Flight Test. Figure 2 shows the time history of the transmitter pulse. For mathematical modeling, the time history has been broken into four segments: the pre-pulse segment, the pulse, the tail, and the ringing. The energy in the time history in various times is given by

$$
\begin{array}{lll}
\text{pre-pulse} & \dfrac{\bar{E}}{E} = 10^{-0.9}\left(\dfrac{t_t}{78\ \mu s} + 1\right) & -78\ \mu s < t < 0 \\
\text{pulse} & \dfrac{\bar{E}}{E} = 1 & t_t = 0 \\
\text{tail} & \dfrac{\bar{E}}{E} = 10^{-0.26} & t_t = \tau \\
\text{ringing} & \dfrac{\bar{E}}{E} = 10^{-1.26e - (t_t - \tau/29\ \mu s)} & 0 < t_t \\
 & \tfrac{1}{2}\cos\left[\dfrac{2\pi}{6.158\ \mu s}\ (t_t - \tau)\right] + 1 &
\end{array}
\qquad (12)
$$

and is computed by the FORTRAN function shown in Attachment 1.

The deconvolution process is shown in Attachment 2. A portion of transformation, $\underline{\underline{E}}$, and its inverse are shown in Figure 6. This figure shows in each case a 50 x 75 segment of the 90 x 90 matrix, with the value of the matrix element encoded in the gray shade. It should be noted that in the display of the matrix itself, all values shown are positive while in the display of the inverse, both positive and negative values are shown.

A set of data which included a measurement of Mt. Shasta was used to evaluate the deconvolution procedure. To account for difficulties in measuring the details of the ringing, a variable phase was included in the cosine term (Equation 12), and different values of phase were tried as shown in Figure 7. In each segment of the figure, the top curve illustrates the time history of the transmitter pulse which was assumed, the middle curve shows the measured signal as a function of range, and the bottom curve shows the result of the deconvolution. Note that an arbitrary time offset has been applied to the top curve. It is interesting to note that no significant variations seem to exist among the six figures shown. To show this in greater detail, three parameters of each figure were plotted as shown in Figure 8. The variations among the different phases are small, and it appears that the best results are obtained at zero phase. In addition to the strong peak in amplitude indicating a return from the mountain at slightly less than 10 km, there is a smaller signal at close range, which may be atmospheric aerosol blown from the mountain into the beam, since the measurement was made slightly downwind of the mountain. After the mountain, a ringing signal still exists, since the deconvolution was apparently not accurate enough to remove this completely.

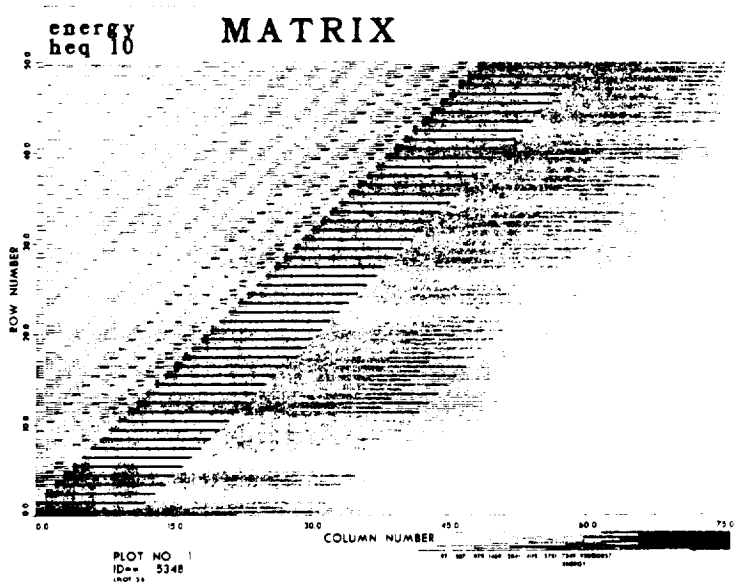

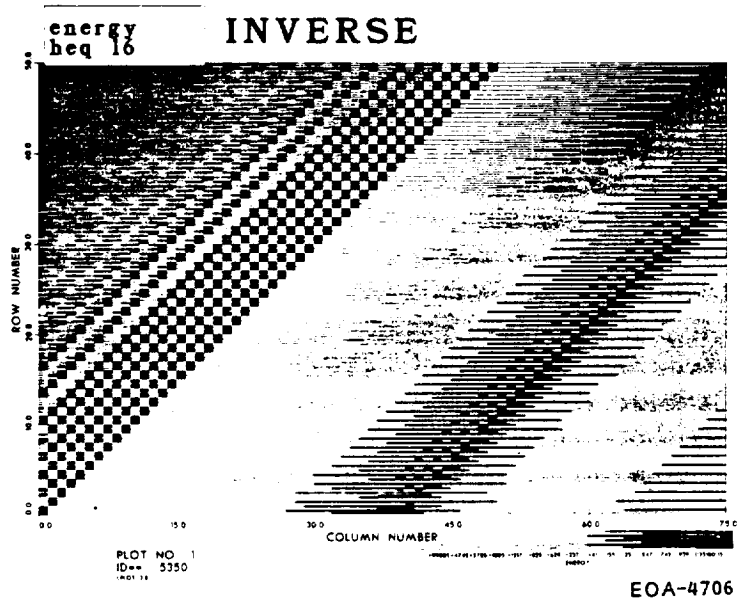

EOA-4706

Figure 6. Matrix and Inverse Displays

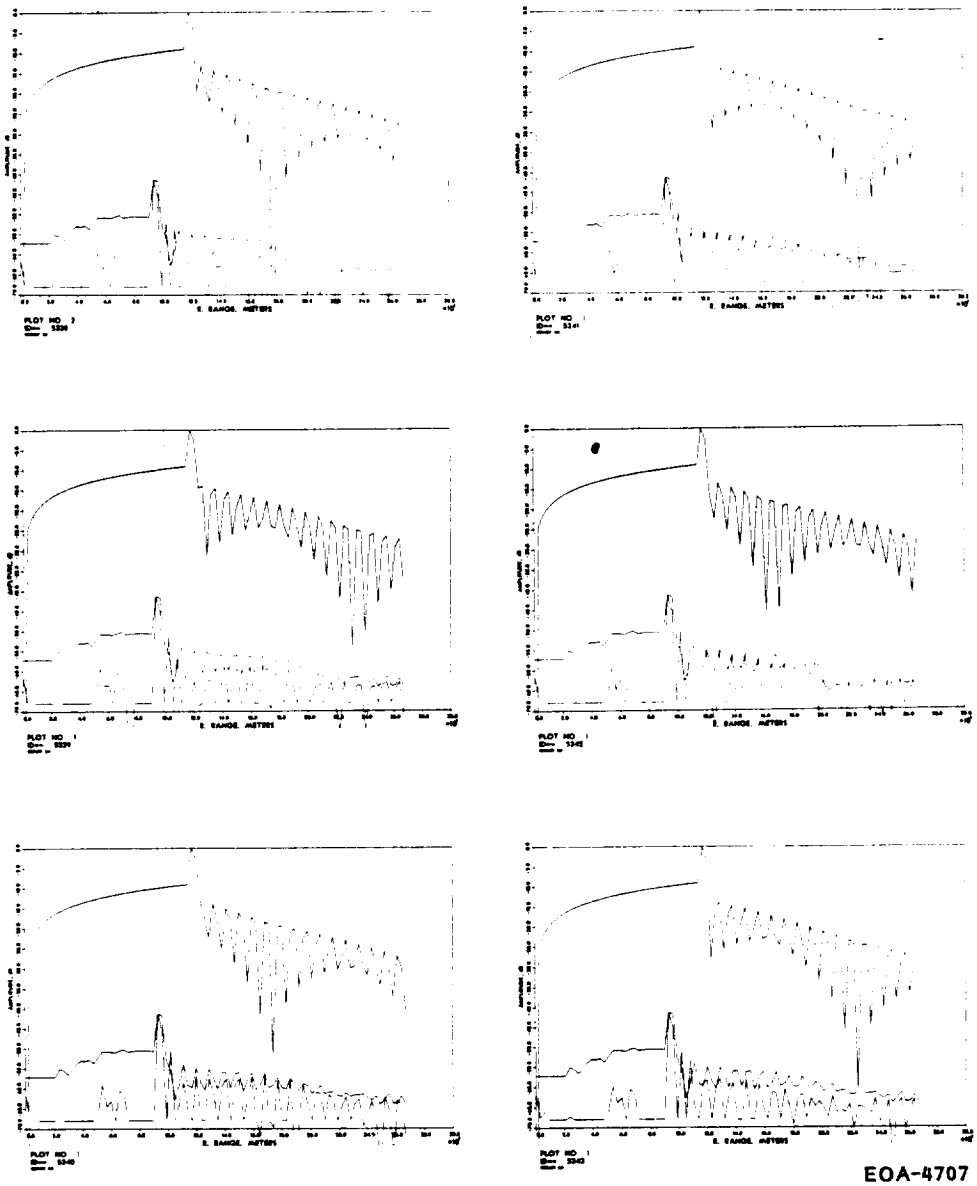

EOA-4707

Figure 7. Mt. Shasta Measurements

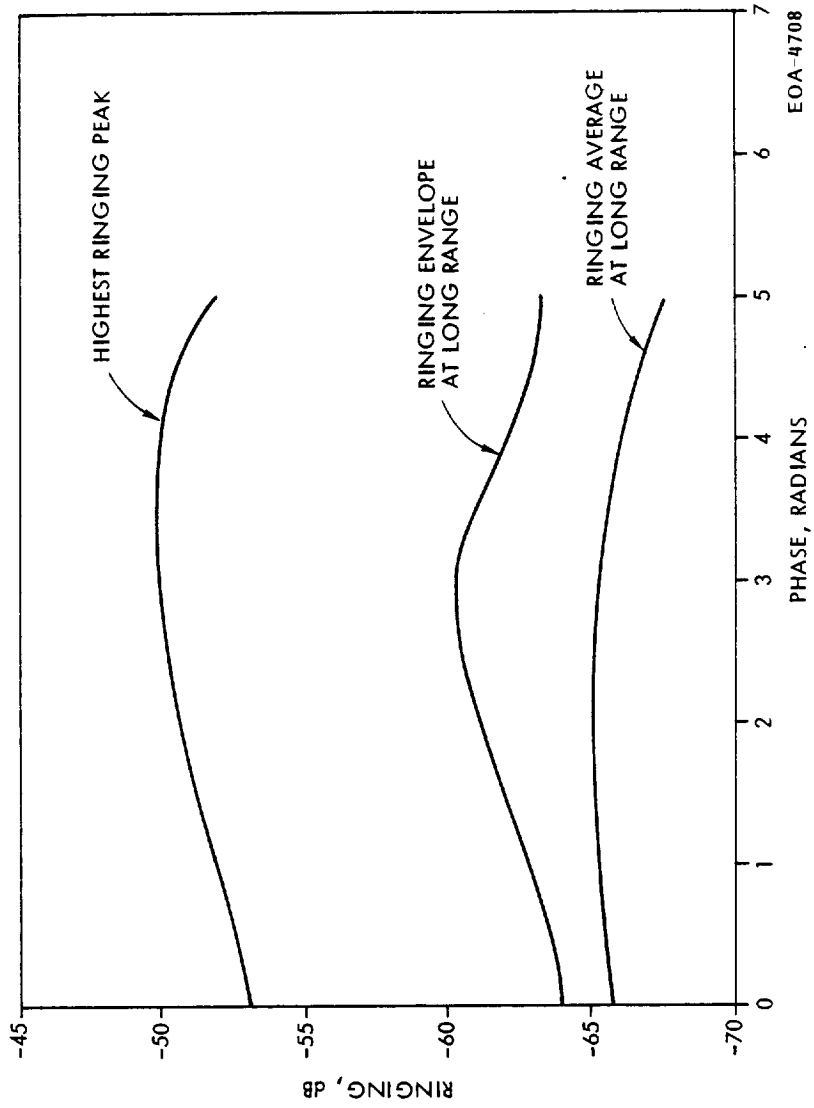

Figure 8. Optimization of Ringing Phase, Flight 10, 1984 SSP

The above example was particularly simple, since the velocity measurements were all nearly the same in a single deconvolution effort. To illustrate a more complicated example, typical of those expected in many of the interesting flow fields, a data set was chosen in which there was a distribution of velocities. In the set selected, most of the velocities did cluster around zero, -1, and +1 meters per second. In this case, Equations 9, 10, and 11 were all plotted in Figure 9. It is reasonably convincing from this figure that a velocity of zero meters per second existed in a region between about 6 and 9 km. Similar plots were constructed for the other two velocities. In addition, one other case needed to be considered: if there existed a velocity at which there was a significant spectral peak which remained just below the measured one at all ranges, it would be possible for this velocity never to appear in the deconvolution process. Thus, one case was run with $\bar{M}_k = \bar{0}$. These results are shown in Figure 10. In principle then, it is possible that the correct velocity for each range gate is never observed. However, one can make convincing continuity arguments that this situation is extremely unlikely. To better illustrate the partial deconvolution process in the case of multiple velocities along a given line of sight, Figure 11 shows several reconstructed spectra from the range sample shown in the previous two figures. Each figure shows four spectra. The top line, which is dotted, shows the peak of the envelope, indicating the highest peak which could possibly exist in the spectrum. The remaining three lines show from top to bottom the maximum expected and minimum signal at each velocity at the range written on the spectrum. At 7.5 km the velocity of 0 meters per second is very believable, due to the peak located there in both the minimum and expected spectrum. A similar, but slightly less convincing, situation exists at 1 meter per second at 6 km and again at -1 meter per second at 9 km. At 19.5 km, all the spectra are considerably lower than they were in the previous cases, and it is unlikely that it is possible to make a valid velocity estimate.

2.2 MODULATOR REFURBISHMENT

Upon receiving the two modulators back from the Marshall Space Flight Center, a number of tests were completed to recharacterize them. In the present Severe Storms system, the first modulator acts as an optical switch and the second as a "tail biter." During the last field test, the "tail biter" was electrically damaged, thus the need arose to reevaluate the modulator performance.

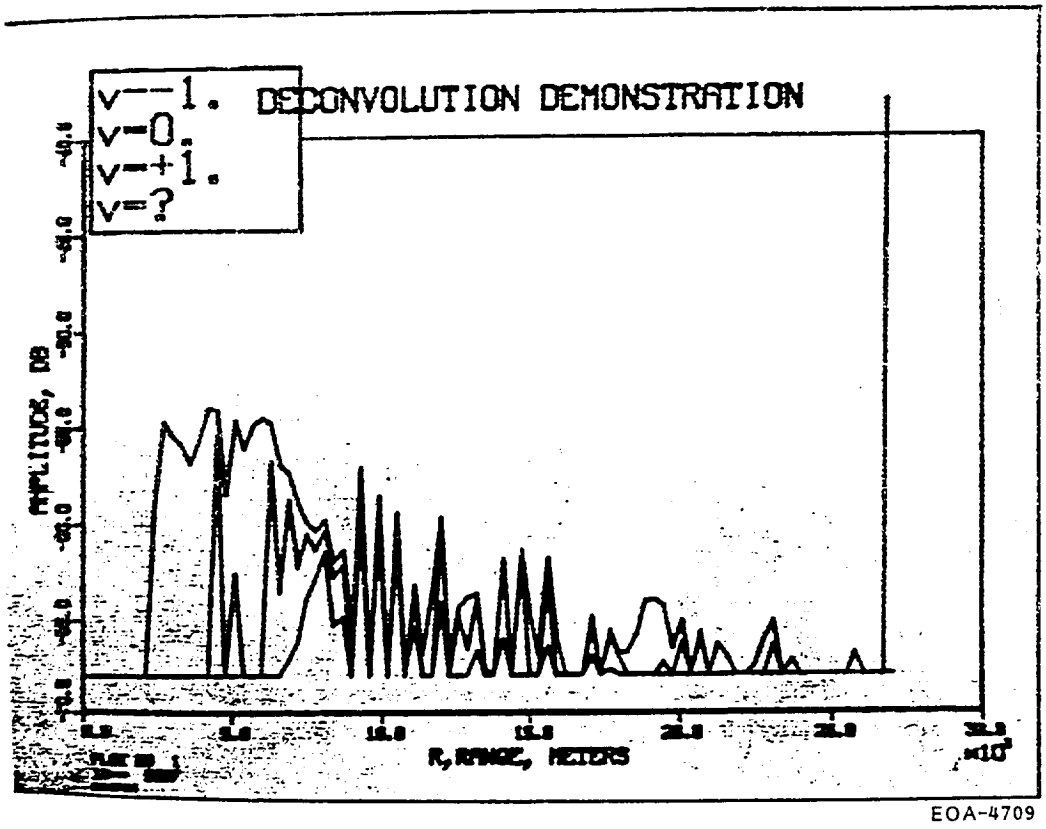

Figure 9. Three Convolutions at Zero Velocity

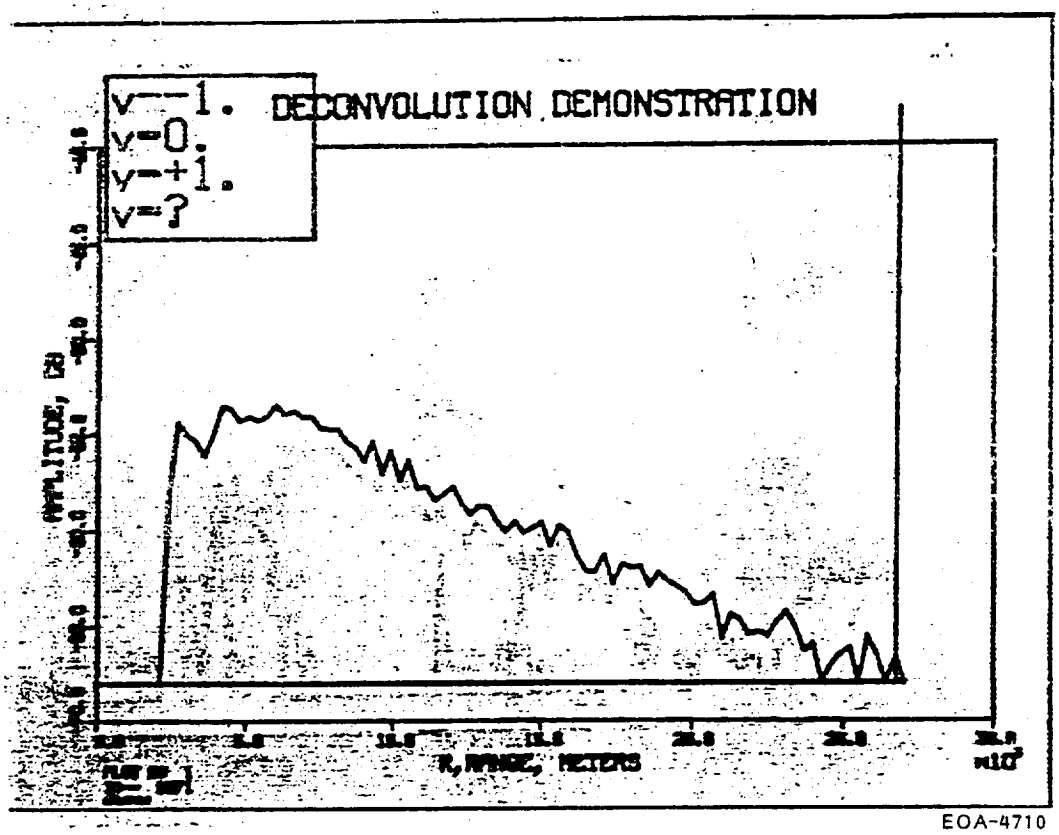

EOA-4710

Figure 10. Envelope of Deconvolution Results

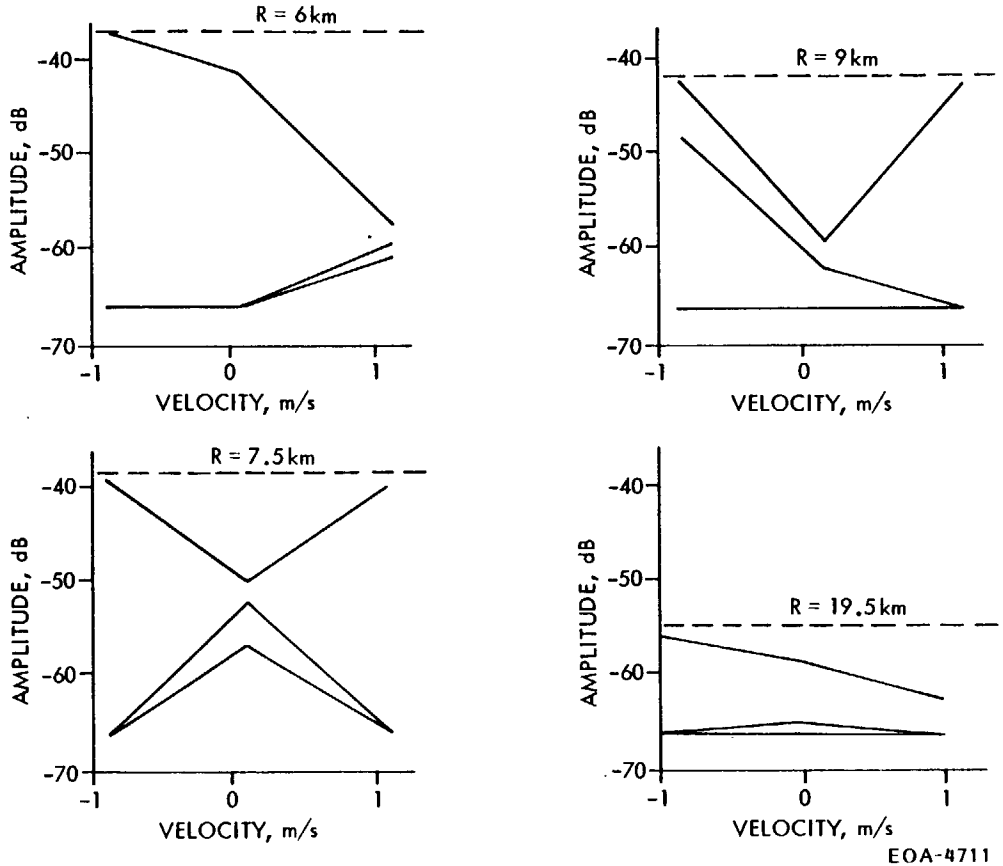

Figure 11. Reconstructed Spectra

The extinction ratio and transmission of the modulators in tandem and also separately were measured. In addition to this, an infrared transmission scan was done.

Upon completion of these experiments, the modulators were tested for optical ringing and the optical pulse height to optical ringing ratio was determined.

The data from these two experiments indicated that two new crystals and modulator housings were needed. The crystals were ordered in April and a mid-November (previously mid-June) delivery is expected. The modulator housings were redesigned and fabricated to optical ringing. The design implemented has been successfully used on other Raytheon programs. Since the new crystals had such a long lead time, the original switching modulator was reworked (end faces repolished). This reworked crystal has been mounted in the new modulator housing and similar tests have been completed. The results of these tests will be summarized and forwarded to MSFC shortly.

2.3 ISOLATOR REFURBISHMENT

New indium antimonide was ordered and received in July. These wafers were polished by Cominco rather than the Research Division at Raytheon because they claimed they could do the work at minimal cost. The material was sliced from the original crystal grown in 1977. Examination of the received wafers indicated that Cominco did not have the skill in polishing as claimed. In addition, there is a surface mark on each wafer on the same face. (Crystals have an antimonide side and an indium side.) The surface mark is a sign of a material inclusion that propagates through the crystal and is therefore found in each slice. Inclusions can have a bad effect on the optical wave front as it passes through the crystal acting in effect as a lens since the index will be different than surrounding material.

Tests are underway to examine the wafers at 10.6 μm.

Old wafer stock, not yet polished, will be polished at Research as soon as blocking stock can be located. New stock will be ordered from Cominco in the raw cut state only.

2.4 IMPROVED CALIBRATION SETUP

There are several problems with the existing internal calibration equipment. The signal-to-noise ratio (SNR) is very sensitive to the tolerance of the wheel placement due to the acute focusing of the present lens. In addition, the wheel-driving motor produces a non-optimum Doppler frequency, and the SNR exceeds the dynamic range of the processor.

An existing 5.5X expander used in reverse would shrink the output beam substantially to give a more narrow focal point.

The wheel will continue to be placed at an angle of incidence of 45° due to the mass of accumulated data already processed at that angle.

The motor, which drives the wheel, should be upgraded to raise the Doppler frequency (f_D) above 3 MHz. A 3.6K rpm motor would produce f_D = 4.087 MHz.

With a speed of 3.6K rpm, a beam size at the target of 4 mm would be required to produce a passband of 100 kHz.

It has been determined that the optimum situation would produce a spot less than 1 mm on the wheel. Therefore, the length of time a particle is in the beam comes into effect to determine the passband. A particle on the disc (at the operating radius of 8.13 cm) will take 4.5×10^{-5} s to pass through the beam, which results in a 22-kHz passband.

2.4.1 RESULTS AND DISCUSSION

A diagram of the modification is depicted in Figure 12, showing the proposed 5.5X expander in reverse and dimensions of the system.

The existing 5.5X expander design is recommended to be manufactured, and a 3.6K rpm closed motor should be purchased.

3. PLANS

A new beam expander will be designed for the local oscillator. A cooperative effort with National Severe Storms Laboratory will begin on evaluating the velocity accuracy.

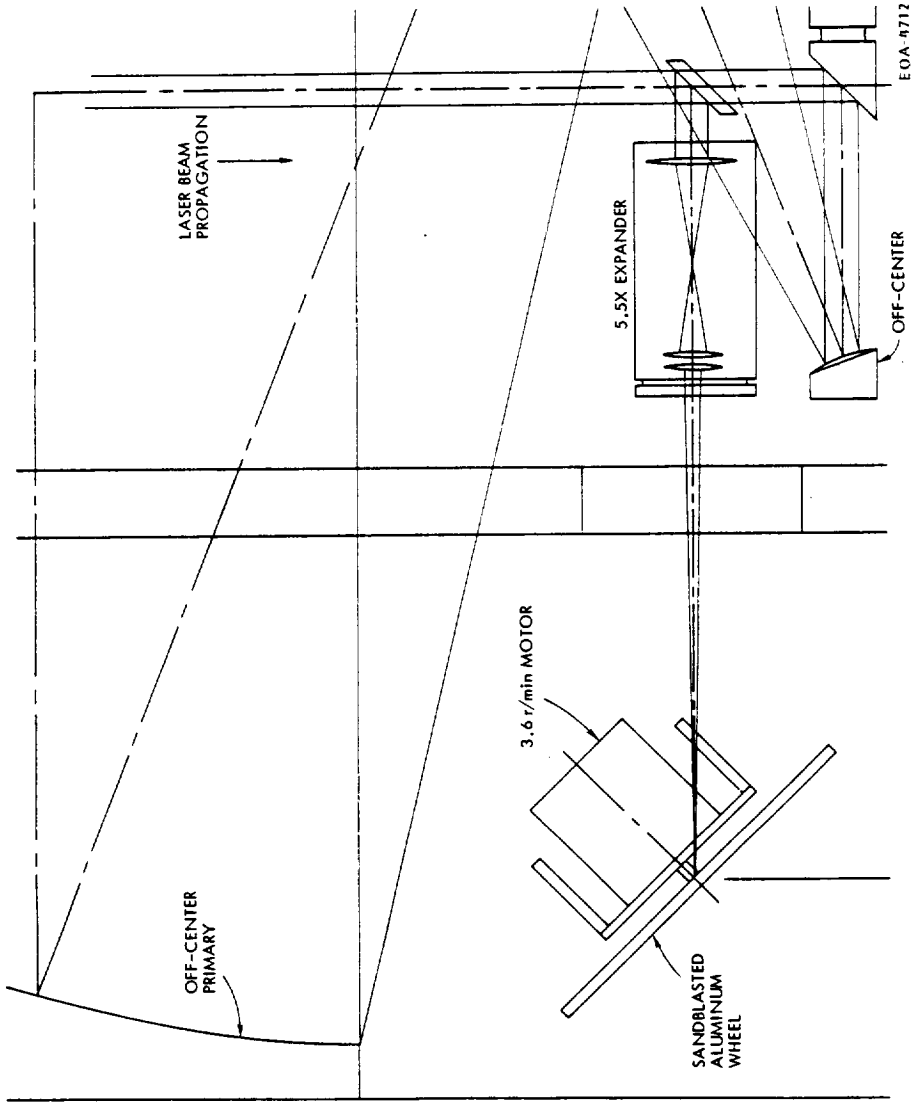

Figure 12. Modified System

At this point, all possible testing and fabrication have been completed. As soon as the new crystals arrive, they will be mounted in their respective modulator housings and individual and tandem testing will be finished.

ATTACHMENT 1


```
      FUNCTION ENERGY(I)
C*****************************************************************
C
C     FUNCTION ENERGY CALCULATES THE ENERGY IN THE SEVERE STORMS
C     TRANSMITTER PULSE DURING THE I-TH TIME 2-MICROSECOND RANGE
C     GATE INTERVAL.  I IS ZERO FOR THE PULSE ITSELF, POSITIVE FOR
C     ANY TIME AFTER THE PULSE, AND NEGATIVE BEFORE THE PULSE.
C
C-----------------------------------------------------------------
C
C     FUNCTIONS AND SUBROUTINES USED:
C                         NONE
C
C
C-----------------------------------------------------------------
C
C     WRITTEN BY CHUCK DIMARZIO ON 14 JANUARY 1985
C
C*****************************************************************
C*****************************************************************
      PI    = ACOS(-1.0)
      TAU   = 2.E-06
      TAIL  = 10.**(-0.26)
      RINGT = 6.152RE-06
      RINCO = 25.E-06
      PRET  = 79.E-006
      PREP  = 10.**(-0.9)
      RINGP = 10.**(-1.26)
C-----------------------------------------------------------------
C
C     TAU IS   THE PULSE LENGTH
C     TAIL IS  THE ENERGY IN THE INTERVAL AFTER THE PULSE
C     PREP IS  THE ENERGY OF THE PRE-PULSE SIGNAL IN THE INTERVAL
C                IMMEDIATELY BEFORE THE PULSE
C     RINGP IS THE ENERGY PEAK OF THE RINGING
C     PRET IS THE LENGTH OF TIME THE PRE-PULSE SHELF LASTS
C     RINGF IS THE PERIOD OF THE RINGING
C     RINGD IS THE DECAY TIME OF THE RINGING TO 1/E
C
C*****************************************************************
C
      IPEC=2.*PI/RINGT
      FI=IPEC*TAU
C*****************************************************************
C     PULSE
C
      ENERGY=1.
      IF(I.EQ.0)RETURN
C*****************************************************************
C     TAIL REGION (ONE GATE)
C
      ENERGY=TAIL
      IF(I.GT.0)RETURN
C*****************************************************************
C     LAST IF ENDS CONDITION
```

ATTACHMENT 1 (Cont'd)

```
FUNCTION ENERGY      74/74   OPT=1  PMD1P                FTN 4.8+507        85/01/17. 15.49.32        PAGE    2

                ENERGY=0.
                TIME =I*DELT/FLOAT(I)
                IF(TIME.GE.5.*RINGO)RETURN
                IF(TIME.LT.-PRET)RETURN
      ******************************************************************
      C         RINGING
      C
                IF(I.GT.1)ENERGY=RINGP*EXP(-(TIME-TAU)/RINGO)*
               1(COS(FREQ*(TIME-TAU))+1.)*0.5
      C*****************************************************************
      C         SIMPLE DEFINE THE PULSE (TRIANGULAR)
      C
                IF(I.LT.0)ENERGY=PREP*(TIME/PRET+1.)
                RETURN
      C*****************************************************************
                END

SYMBOLIC REFERENCE MAP (R=3)

ENTRY POINTS      DEF LINE      REFERENCES
    4  ENERGY         1            47       54        60        61        71

VARIABLES      SN  TYPE          RELOCATION
   105  ENERGY     REAL                            DEFINED    48       53        58       65        70
   116  FREQ       REAL                              REFS     44       65     DEFINED     43
   117  FT       * REAL                            DEFINED    45
     0  I          INTEGER               F.P.        REFS     49       54        59       65        70
                                                   DEFINED     1
   106  PI         REAL                              REFS     43    DEFINED      21
   114  PREP       REAL                              REFS     70    DEFINED      27
   113  PRET       REAL                              REFS     61       70     DEFINED     26
   112  RINGO      REAL                              REFS     60       65     DEFINED     25
   115  RINGP      REAL                              REFS     65    DEFINED      28
   111  RINGT      REAL                              REFS     43    DEFINED      24
   110  TAIL       REAL                              REFS     53    DEFINED      23
   107  TAU        REAL                              REFS     44       59       2*65    DEFINED     22
   120  TIME       REAL                              REFS     60       61       2*65      70     DEFINED     59

EXTERNALS           TYPE    ARGS           REFERENCES
        ACOS        REAL       1 LIBRARY      21
        COS         REAL       1 LIBRARY      69
        EXP         REAL       1 LIBRARY      65

INLINE FUNCTIONS    TYPE    ARGS        DEF LINE   REFERENCES
        FLOAT       REAL       1  INTRIN               59

STATISTICS
  PROGRAM LENGTH                 121B        81
```


ORIGINAL PAGE IS
OF POOR QUALITY

Raytheon

ATTACHMENT 2


```
      SUBROUTINE DIACON(S,F)
      DIMENSION E(90,90),F(90),L(90),M(90),S(90)
C*****************************************************************
C
C     SUBROUTINE DIACON PERFORMS A DECONVOLUTION OF THE DATA FROM A
C     SINGLE SCAN OF THE SEVERE STORMS SYSTEM.  IT ASSUMES THAT IT
C     WILL RECEIVE 90 AMPLITUDES, ALL ASSOCIATED WITH THE SAME
C     VELOCITY.  THE INPUT, S, AND OUTPUT, F, ARE 90-ELEMENT VECTORS.
C
C     L AND M ARE WORKING ARRAYS FOR THE MATRIX INVERSION OF THE
C     IMSL LIBRARY.
C
C     ENERGY IS THE FUNCTION WHICH CALCULATES THE PULSE ENERGY
C     AT A TIME GIVEN BY AN INTEGER NUMBER OF RANGE GATES AFTER
C     THE PULSE (THIS TIME MAY BE NEGATIVE)
C
C-----------------------------------------------------------------
C
C     SUBROUTINES CALLED: FUNCTION ENERGY
C
C-----------------------------------------------------------------
C
C     WRITTEN BY CHUCK DIMARZIO  16 JANUARY 1985
C
C*****************************************************************
C*****************************************************************
C
C     FIRST CALCULATE THE E MATRIX OF ENERGY VALUES
C
      DO 20 NR=1,90
      DO 10 NG=1,90
C
C     NR IS THE RANGE INTEGER
C     NG IS THE TIME INTEGER FOR THE RANGE GATE
C
      E(NR,NG)=ENERGY(NG-NR)
   10 CONTINUE
   20 CONTINUE
C
C*****************************************************************
C
C     INVERT THE MATRIX
C
      CALL LINV1(E,90,0,L,M)
C
C*****************************************************************
C
C     CALCULATE THE ORIGINAL VECTOR
C
C-----------------------------------------------------------------
C
C     LOOP FOR EACH ELEMENT
C
      DO 40 KK=1,90
C
C     SET THE ELEMENT
C
```

```
      F(I)=0.
C
C.......................................................................
C
C     LOOP TO SUM OVER ALL COLUMNS OF THIS ROW OF E-INVERSE
C
      DO 30 NG=1,9L
      F(NR)=F(NR)+E(NC,NR)*S(NG)
   30 CONTINUE
C
C     END OF SUMMING LOOP
C
C.......................................................................
C
   40 CONTINUE
C
C     END OF ELEMENT LOOP
C-----------------------------------------------------------------------
C
      RETURN
C***********************************************************************
      END
```

SYMBOLIC REFERENCE MAP (R=3)

```
ENTRY POINTS    DEF LINE     REFERENCES
  3 DEARON          1           77

VARIABLES     SN  TYPE              RELOCATION
   61  D       *  REAL                         REFS     44
   62  E          REAL      ARRAY              REFS      2     44      45  DEFINED     36
    0  F          REAL      ARRAY     F.P.     REFS      2     65  DEFINED       1     58     65
17726  L          INTEGER   ARRAY              REFS      2     44
20060  M          INTEGER   ARRAY              REFS      2     44
   60  NG         INTEGER                      REFS   2*36   2*65  DEFINED      31     64
   57  NR         INTEGER                      REFS   2*36     58    3*65  DEFINED     30     54
    0  S          REAL      ARRAY     F.P.     REFS      2     65  DEFINED       1

EXTERNALS        TYPE     ARGS       REFERENCES
   ENERGY        REAL       1           36
   MINV                     5           44

STATEMENT LABELS              DEF LINE   REFERENCES
   0  10                         37         31
   0  20                         39         30
   0  30                         65         64
   0  40                         7?         54

LOOPS  LABEL   INDEX    FROM-TO   LENGTH   PROPERTIES
   7   20      NE       30  58     149           EXT REFS  NOT INNER
  1?   1?      NC       31  ?7     113           EXT REFS
  2?   4?      NG       ?4  7?     16B           NOT INNER
  3?   3?      NC       65  ??      3B      INSTACK
```